Journal of
**Applied Crystallography**
ISSN 0021-8898

Received 1 February 2006
Accepted 17 July 2006

# Inferring orientation distributions in anisotropic powders of nano-layered crystallites from a single two-dimensional WAXS image

**Yves Méheust,[a]* Kenneth Dahl Knudsen[b] and Jon Otto Fossum[a]**

[a]Physics Department, Norwegian University of Science and Technology, 7491 Trondheim, Norway, and [b]Physics Department, Institute for Energy Technology, Kjeller, Norway. Correspondence e-mail: meheust@phys.ntnu.no

The wide-angle scattering of X-rays (WAXS) by anisotropic powders of nano-layered crystallites (nano-stacks) is addressed. Assuming that the orientation distribution probability function $f$ of the nano-stacks only depends on the deviation of the crystallites' orientation from a fixed reference direction, a relation providing $f$ from the dependence of a given diffraction peak's amplitude on the azimuthal angle is derived. The method is applied to two systems of sodium fluorohectorite (NaFH) clay particles, using synchrotron radiation and a WAXS setup with a two-dimensional detector. In the first system, which consists of dry-pressed NaFH samples, the orientation distribution probability function corresponds to a classical uniaxial nematic order. The second system is observed in bundles of polarized NaFH particles in silicon oil; in this case, the nano-stacks have their directors, on average, in a plane normal to the reference direction, and $f$ is a function of the angle between a nano-stack's director and that of the plane. In both cases, a suitable Maier–Saupe function is obtained for the distributions, and the reference direction is determined with respect to the laboratory frame. The method only requires one scattering image. Consistency can be checked by determining the orientation distribution from several diffraction peaks independently.



## 1. Introduction

The recording of a powder diffraction signal using a two-dimensional detector is a potentially simple and efficient technique for determining characteristic structural length scales in crystals. The basis of the technique is that a scattering volume containing an isotropic powder consisting of a large number of particles with identical crystalline structure offers to the incoming beam all possible incidence orientations with respect to the crystallites. Consequently, all the diffraction peaks characteristic of the crystallite structure are visible in any of the azimuthal planes, and all azimuthal planes are equivalent: a simple scan of the scattering angle, $2\theta$, in a given azimuthal plane, provides a spectrum containing peaks at all structural length scales characteristic of the crystallites, apart from those that are extinct due to form-factor effects. The scattering image collected by a two-dimensional detector is isotropic, and its centre of symmetry denotes the direction of the incident beam. Radial cuts of the images passing through this centre provide identical one-dimensional spectra that can be averaged over all azimuthal angles in order to increase the signal to noise ratio significantly.

It is well known that reconstruction of the three-dimensional crystal structure from powder data is made difficult by the overlapping of reflections with similar diffraction angles. The interpretation is fairly easy in the case where only a dominant feature of the structure is investigated. A particular case is that of nano-layered systems, where the powder is made of particles, or clusters of particles, that consist of a stack of identical quasi-two-dimensional crystallites. The Bragg reflections resulting from the set of Bragg planes associated with those stacks are the most intense and can be interpreted in quite a straightforward manner. A number of natural (vermiculite, montmorillonite) and synthetic (fluorohectorite) smectite clays present, in weakly hydrated states, a microstructure in which particles are platelet-shaped and nano-layered. The repeating crystallite is a silicate platelet, of 1 nm thickness, and the stacks are held together by cations shared between adjacent platelets. The stacks can swell by intercalation of ions and molecules (water, in particular), and powder diffraction has been used extensively to study that swelling, both on natural (Wada *et al.*, 1990) and synthetic (da Silva *et al.*, 2002) smectite clays.

A wide range of natural or man-made materials are aggregates of crystallites with the same crystallographic structure. The distribution of the crystallite orientations inside the material is rarely isotropic, hence their X-ray diffraction signal is that of an anisotropic powder. Many examples of such polycrystalline aggregates can be found among metals. The analysis from X-ray diffraction data of the preferred crystal-

lographic orientations in those metals, *i.e.* their texture, provides information on the history of their deformation (Wenk, 1985), as it does for rocks, another type of polycrystalline materials with a larger degree of complexity (several types of crystals coexist). This is done by decomposing the distribution of the reflections' intensities as a function of the angular direction into a superposition of distributions resulting from single reflections (pole figures), and subsequently inferring the orientation distribution probability (ODP) for the crystallites. Several general methods (Wenk, 1985; Bunge, 1993) have been developed to tackle that potentially difficult (and sometimes, non-univocal) inversion. From the experimental point of view, two-dimensional detectors have proved useful in such texture analyses, as they allow gathering of the data necessary to the pole-figure analysis in a short time and without changing the sample position (Ischia *et al.*, 2005). For the practical applicability of such methods, see the work of Wenk & Grigull (2003). Note that texture studies have recently found an interesting application in methods to determine the complete three-dimensional structure of a crystal from anisotropic powder diffraction data collected from samples with different textures (Lasocha & Schenk, 1997; Wessels *et al.*, 1999).

The study of preferential orientation in polycrystalline materials consisting of nano-layered particles (quasi-one-dimensional crystals), such as the clays presented above, has made little use of the general inversion technique for texture data, since there is basically no overlap of pole figures for those materials. In the case where the ODP possesses an axial symmetry, it is classically determined experimentally by measuring a rocking curve, where the sample is rotated around an incidence angle $\theta$ corresponding to a well known $00k$ reflection, and the scattered intensity is measured at the diffraction angle $2\theta$ as a function of $\theta$ (Güntert & Cvikevich, 1964; Taylor & Norrish, 1966). In this paper, we present an alternative method for determining the orientation distribution from the scattering data for the case in which it only depends on one characteristic angle. When the assembly of nano-stacks presents a partial privileged orientation, all azimuthal planes are no longer equivalent. Our method is based on monitoring the dependence of the intensity of a given reflection peak on the azimuthal angle. It can thus be carried out on a single two-dimensional wide-angle scattering image. In other words, we monitor the anisotropy of that image at a given reflection. Note that monitoring of the intensity along Debye rings has previously been done in a similar manner for cubic and hexagonal materials (Puig-Molina *et al.*, 2003; Wenk & Grigull, 2003). We do not address the influence of the ODP on the diffraction profiles in a given azimuthal plane, a problem to which much attention has been given in the past for systems like pyrolytic graphite (Güntert & Cvikevich, 1964) and smectite clays (de Courville *et al.*, 1979; Plançon, 1980).

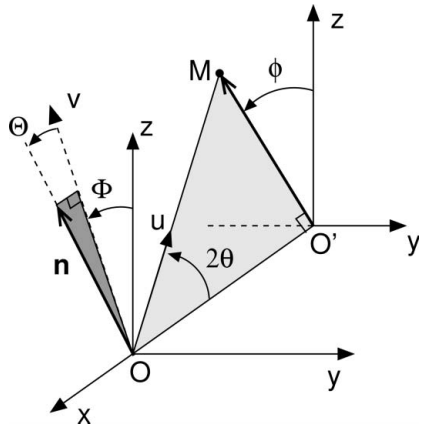


**Figure 1**
In the laboratory frame (**x**, **y**, **z**) (with **x** parallel to the incident beam), the angular direction of the diffracted beam, denoted by point $M$ in the detector plane $\mathbf{y}O'\mathbf{z}$, is defined by the scattering angle $2\theta$ and the azimuthal angle $\varphi$. The area shaded in light gray denotes the plane containing the incident and diffracted beams; it is normal to the $\mathbf{y}O\mathbf{z}$ plane and makes an angle $\varphi$ with the $\mathbf{z}O\mathbf{x}$ plane. The dark gray area also denotes a plane normal to the $\mathbf{y}O\mathbf{z}$ plane and makes an angle $\Phi$ with the $\mathbf{z}O\mathbf{x}$ plane. It is used to define the orientation of the director **n** of a given crystallite with respect to the fixed frame, according to the angles $\Theta$ and $\Phi$.

The paper is organized as follows. In section §2, we present the theoretical background of the method, for both geometries. The method is then applied to data from two experiments corresponding to two geometrical configurations observed in systems of the synthetic smectite clay Na fluorohectorite (in sections §3 and §4, respectively). In §5, we discuss the points of interest of the method.

## 2. Theoretical background

We consider a clay sample placed at the origin $O$ of the laboratory frame $(O, \mathbf{x}, \mathbf{y}, \mathbf{z})$ (see Fig. 1). An incident X-ray beam parallel to **x**, and of wavelength $\lambda$, is scattered by the sample, and the scattered intensity is recorded in a detector plane $\mathbf{y}O'\mathbf{z}$, $O'$ being the point where the direct beam would hit the detector in the absence of a beamstop behind the sample. The running point $M$ on the detector is denoted by the direction of the line $O\mathbf{u}$ passing through the points $O$ and $M$; the corresponding angular frame consists of the scattering angle $2\theta$ and the azimuthal angle $\varphi$.

The sample consists of a population of nano-layered crystallites containing $\sim$100 stacked identical layers. In what follows, we shall only consider the scattering by these one-dimensional crystals. Therefore, the orientation of each crystallite needs to be denoted by only one vector, the common director **n** of the crystallite's stacked layers. We assume that the ODP function $f$ for the population of directors depends only on a single angle $\alpha$, which is the angle between a crystallite's director **n** and a reference orientation $\mathbf{n}_0$. Readers familiar with the notations conventional in texture analysis can think of $\mathbf{n}_0$ as the sole vector relevant to the definition of a sample frame in our geometry, and similarly of **n** as the sole vector relevant to the definition of the crystal frame for each crystallite. The density probability function is normalized with respect to the total solid angle available to the description, *i.e.*

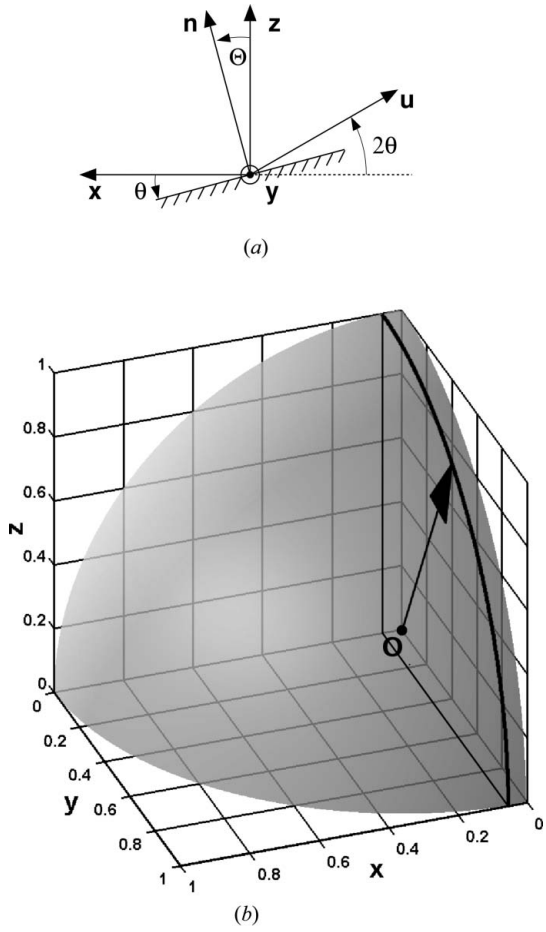


**Figure 2**
(*a*) The condition of specular reflection on the Bragg planes requests that $\Theta = \theta$, as sketched here in the $\mathbf{x}O\mathbf{u}$ plane. (*b*) The thick curve is that described on the unit sphere by the end of vector $\mathbf{n}$ (director of the scatterer) as the azimuthal position of the diffracted beam, $\varphi$, varies between 0 and $\pi/2$. Here the scattering angle $2\theta$ corresponds to the Bragg reflection (002) on a nano-layered Na fluorohectorite particle in the hydration state 1WL, with $\lambda = 0.71$ Å.

$$\int_0^{2\pi}\int_0^{\pi/2} f(\alpha)\sin\alpha\,\mathrm{d}\alpha\,\mathrm{d}\beta = 1, \qquad (1)$$

where $(\alpha, \beta)$ is a standard spherical angular frame, and $\alpha$ is considered in the range $[0; \pi/2]$ because $\mathbf{n}$ and $-\mathbf{n}$ are equivalent in terms of nano-stack orientation.

The ODP function $f$ possesses an axial symmetry around $\mathbf{n}_0$, but is not isotropic. Its anisotropy results in an anisotropic distribution of the scattered intensities in the detector plane.

### 2.1. Diffraction by an anisotropic distribution of nano-stacks

The orientation of each crystallite director $\mathbf{n}$ with respect to the laboratory frame is denoted by the angular frame $(\Theta, \Phi)$ (see Fig. 1), with $\Theta$ in the range $[0; \pi/2]$ and $\Phi$ in the range $[-\pi; \pi]$. $\Theta$ is the angle between the crystallite's director and the plane $\mathbf{y}O\mathbf{z}$, while $\Phi$ is the azimuthal angular coordinate of the director.

Let us first consider a single crystallite whose stacking planes make an angle $\theta$ with the incident beam, corresponding to the Bragg condition for the stack. This implies that it mostly scatters along the direction $O\mathbf{u}$, *i.e.* that the azimuthal direction for scattering is $\varphi = \Phi$, and the scattering angle is $2\theta = 2\Theta$ (see Fig. 2*a*). As the azimuth $\varphi$ describes the $[-\pi; \pi]$ range, the trajectory on the unit sphere of the director for the crystallites that scatter along that azimuth describes a circle in the plane $x = \sin\theta$ (see Fig. 2*b*). This director is therefore defined in the frame $(\mathbf{x}, \mathbf{y}, \mathbf{z})$ by the coordinates

$$\mathbf{n}_{2\theta}(\varphi) = \begin{pmatrix} \sin\theta \\ -\cos\theta\sin\varphi \\ \cos\theta\cos\varphi \end{pmatrix}. \qquad (1)$$

Next, we consider the whole crystallite population, and we assume that their size and orientation distributions are uncorrelated and that the beam defines a scattering volume that is large enough for the size distribution of the scatterers to be entirely contained in it. Hence, we assume that the amplitude of a diffraction peak in the direction $(2\theta, \varphi)$ is proportional to the number of scatterers that satisfy the Bragg condition for that direction, and that the proportionality constant is independent of $\varphi$. This also assumes that the scattering peak is well separated from other peaks along the $2\theta$ line. We denote $I_{2\theta}(\varphi)$ as the amplitude of the diffraction peak at scattering angle $2\theta$ and at a given azimuthal angle value $\varphi$, and $\alpha_{2\theta}(\varphi)$ as the angle between the reference director $\mathbf{n}_0$ and that of the crystallites that diffract in the $(2\theta, \varphi)$ direction. The intensity $I_{2\theta}(\varphi)\,\Delta\varphi$ along a length $\Delta\varphi$ of the angular scattering cone of half-opening $2\theta$ is proportional to the quantity $f[\alpha_{2\theta}(\varphi)]\,\Delta\alpha(\varphi, \Delta\Phi)$, where the angular length $\Delta\alpha$ is that travelled by $\mathbf{n}$ on the unit sphere as $\varphi$ describes the range $\Delta\varphi$. The trajectory in Fig. 2(*b*) is travelled at constant speed when varying $\varphi$ uniformly, as appears from the vector $\mathrm{d}\mathbf{n}/\mathrm{d}\varphi$ having a norm $\cos\theta$ [computed from equation (2)], and thus independent of $\varphi$. Therefore, $\Delta\alpha$ only depends on $\Delta\varphi$, which yields

$$I_{2\theta}(\varphi)\Delta\varphi \propto f[\alpha_{2\theta}(\varphi)]\,\Delta\alpha(\Delta\varphi). \qquad (3)$$

Consequently, a uniform sampling of the azimuthal profile of a WAXS peak in the scattering figure is directly related to the orientation distribution for the scatterers, $f$. In particular, a constant profile corresponds to a uniform angular distribution of the platelets, *i.e.* the scattering figure of an isotropic clay powder is isotropic, as expected.

The angle $\alpha_{2\theta}(\varphi)$ can be computed from its cosine, which equals $\mathbf{n}_0 \cdot \mathbf{n}_{2\theta}(\varphi)$. The orientation with respect to the laboratory frame of the mean director $\mathbf{n}_0$ is defined by the angles $\Theta_0$ and $\Phi_0$, and thus its coordinates in the $(\mathbf{x}, \mathbf{y}, \mathbf{z})$ frame are

$$\mathbf{n}_0 = \begin{pmatrix} \sin\Theta_0 \\ -\cos\Theta_0\sin\Phi_0 \\ \cos\Theta_0\cos\Phi_0 \end{pmatrix}. \qquad (4)$$

Thus,

$$\alpha_{2\theta}(\varphi) = \mathrm{acos}\left[\sin\theta\,\sin\Theta_0 + \cos\theta\,\cos\Theta_0\cos(\varphi - \Phi_0)\right]. \qquad (5)$$

For a uniform sampling of the azimuthal scattering intensity profile $I_{2\theta}(\varphi)$, one can directly relate the function $I_{2\theta}(\varphi)$ and $f(\alpha)$, bringing together equations (3) and (5) according to

$$I_{2\theta}(\varphi) \propto f\left\{\text{acos}\left[\sin\theta\,\sin\Theta_0 + \cos\theta\,\cos\Theta_0\,\cos(\varphi - \Phi_0)\right]\right\}. \quad (6)$$

From a given functional form for the distribution $f$, with a given set of shape parameters (peak position, width, reference level), it is possible to fit a function in the form (6) to the experimental data, and infer both the distribution's shape parameters and the reference orientation $\mathbf{n}_0(\Theta_0, \Phi_0)$. The obtained parameters are independent of the particular reflection ($2\theta$ or $q$) chosen, which provides an interesting way of checking the consistency of the results.

### 2.2. Two particular geometries

**2.2.1. Uniaxial nematic configuration**. In the classical uniaxial nematic geometry, the reference orientation is the mean orientation for the population of nano-stacks. The smaller $\alpha$ is, the more crystallites have their orientation along $\mathbf{n}(\alpha)$. The orientation distribution $f$ peaks at 0 and monotonically decreases to its minimum $f(\pi/2)$. An order parameter (de Gennes & Prost, 1993), defined as

$$S = \tfrac{1}{2}\langle 3\cos^2\alpha - 1\rangle_f, \quad (7)$$

*i.e.*

$$S = \pi \int_0^{\pi/2} (3\cos^2\alpha - 1) f(\alpha)\sin\alpha\,\mathrm{d}\alpha, \quad (8)$$

quantifies the overall alignment of the crystallites. For $S = 0$, the population is completely isotropic, while for $S = 1$, all crystallites are perfectly aligned. The alignment can also be quantified in terms of the root mean square (RMS) half-width $w_f/2$ of the distribution, according to

$$\left(\frac{w_f}{2}\right)^2 = \langle\alpha^2\rangle_f = 2\pi \int_0^{\pi/2} \alpha^2 f(\alpha)\sin\alpha\,\mathrm{d}\alpha. \quad (9)$$

**2.2.2. Uniaxial antinematic configuration**. In the configuration that we denote 'antinematic', the crystallites have their directions, on average, in a plane perpendicular to the reference direction. In other words, the stacking planes of the crystallites contain the reference direction, on average. The distribution $f$ peaks around $\pi/2$, monotonically increasing with $\alpha$ from its minimum value $f(0)$. By analogy with the nematic description, an order parameter can be defined, according to

$$S = \left\langle 3\cos^2\left(\frac{\pi}{2} - \alpha\right) - 2\right\rangle_f = \langle 3\sin^2\alpha - 2\rangle_f, \quad (10)$$

*i.e.*

$$S = 2\pi \int_0^{\pi/2} (3\sin^2\alpha - 2) f(\alpha)\sin\alpha\,\mathrm{d}\alpha, \quad (11)$$

and an RMS angular half-width according to

$$\left(\frac{w_f}{2}\right)^2 = \left\langle\left(\frac{\pi}{2} - \alpha\right)^2\right\rangle_f, \quad (12)$$

*i.e.*

$$\left(\frac{w_f}{2}\right)^2 = 2\pi \int_0^{\pi/2} \left(\frac{\pi}{2} - \alpha\right)^2 f(\alpha)\sin\alpha\,\mathrm{d}\alpha. \quad (13)$$

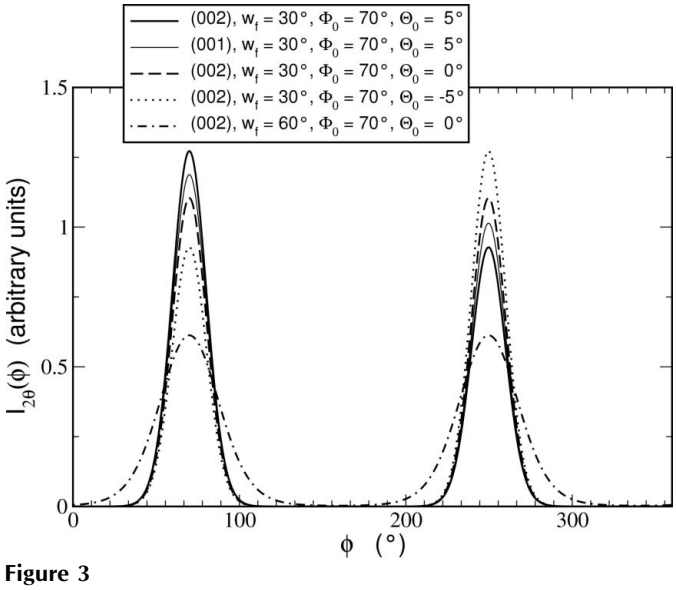


**Figure 3**
Computed profiles describing how the intensity of a given diffraction peak (*i.e.* at a given scattering angle $2\theta$) depends on the azimuthal angle for a population of crystallites with a nematic orientational ordering. The computation was performed for various values of the orientation ($\Theta_0$, $\Phi_0$) of the main director with respect to the fixed frame of the laboratory, and of the width $w_f$ of the nematic angular distribution of the scatterers' directors. Two values of the scattering angle, $2\theta = 3.29^\circ$ (001) and $6.58^\circ$ (002), were used, which means that two diffraction peaks corresponding to two different orders of the same reflection were used.

### 2.3. Modelled azimuthal profiles

Fig. 3 shows expected azimuthal profiles, computed from equation (6), in the case of a nematic geometry where the distribution $f$ is of the classical Maier–Saupe form observed in uniaxial nematic liquid crystals (Maier & Saupe, 1958, 1959):

$$f(\alpha) \propto \exp(m\cos^2\alpha). \quad (14)$$

For a reflection corresponding to a particular value of the scattering angle $2\theta = 6.54^\circ$, two values of the distribution's angular width $w_f$ (30 and $60^\circ$), and three different orientations of the mean director $\mathbf{n}_0$ ($\Theta_0 = -5$, 0 and $5^\circ$) have been used. The profiles are normalized to an integral value 1 over the whole azimuthal range. A profile corresponding to $\Theta_0 = 5^\circ$ for $2\theta = 3.29^\circ$ is also shown.

Fig. 3 shows clearly how the parameters describing the orientational ordering of the crystallites translate into the azimuthal dependence of a diffraction peak's intensity. The angular width of the orientation distribution controls the width of the profile's peaks. The azimuthal coordinate of the mean director, $\Phi_0$, only has the effect of translating the profile along the $\varphi$ scale, while $\Theta_0$ is responsible for the curve's

asymmetry with respect to the azimuth $\varphi = \Phi_0 + 90^\circ$, or, equivalently, the asymmetry of the two-dimensional diffractogram with respect to the plane **x***O***y** (see Fig. 1). In addition, the magnitude of this asymmetry depends on the value of $2\theta$: if there is asymmetry (*i.e.* if $\Theta_0 \neq 0$), it shall be more pronounced for the higher-order peaks of a given reflection.

## 3. Application to a nematic geometry

### 3.1. Fluorohectorite, a synthetic smectite clay

Fluorohectorite belongs to the family of smectite (or swelling 2:1) clays, whose base structural unit is a phyllosilicate platelet, of 1 nm thickness, consisting of two inverted silicate tetrahedral sheets that share their apical O atoms with a tetrahedral sheet sandwiched between (Velde, 1992). Fluorohectorite has a chemical formula per unit cell of $X_x(Mg_{3-x}Li_x)Si_4O_{10}F_2$. Substitutions of $Li^+$ for $Mg^{2+}$ in part of the fully occupied octahedral sheet sites are responsible for a negative surface charge along the platelets. This results here in a large surface charge, 1.2 e (Kaviratna *et al.*, 1996) (as opposed to 0.4 e for the synthetic smectite clay laponite), allowing the platelets to stack by sharing an intercalated cation $X$, for example $Na^+$, $Ni^{2+}$, $Fe^{3+}$. The resulting nano-stacks remain stable in suspension, even at low ionic strength of the solvent, and are therefore present both in water solutions, gels (DiMasi *et al.*, 2001) and weakly hydrated samples (Knudsen *et al.*, 2004).

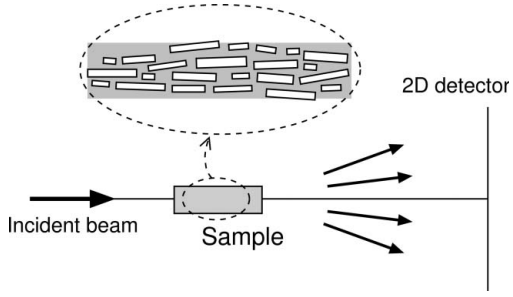


**Figure 4**
Side-view of the experimental scattering geometry used to scatter X-rays by dry-pressed fluorohectorite samples. The inset shows a two-dimensional cut of the sample with the nano-layered crystallites aligned, on average, along a plane close to the horizontal.

Wide-angle X-ray scattering of gel (DiMasi *et al.*, 2001) and weakly hydrated (da Silva *et al.*, 2002) samples of Na fluorohectorite (*i.e.* $X = Na^+$), have shown that the characteristic platelet separation is well defined, and varies stepwise as a function of the surrounding temperature and humidity (da Silva *et al.*, 2003). Samples are anisotropic, but the widths of the corresponding WAXS peaks allows the typical nano-stack thickness to be inferred, which is about 80–100 platelets. This thickness is significantly larger than thicknesses ($< \sim 20$ platelets) for which asymmetry and irrationality in the 00*k* reflections are known to occur (Drits & Tchoubar, 1990), which makes the analysis of 00*k* peaks in powder diffraction spectra of Na fluorohectorite relatively easy.

### 3.2. Dry-pressed samples of Na fluorohectorite

Dry-pressed samples of Na fluorohectorite were prepared from raw fluorohectorite powder purchased from Corning Inc.

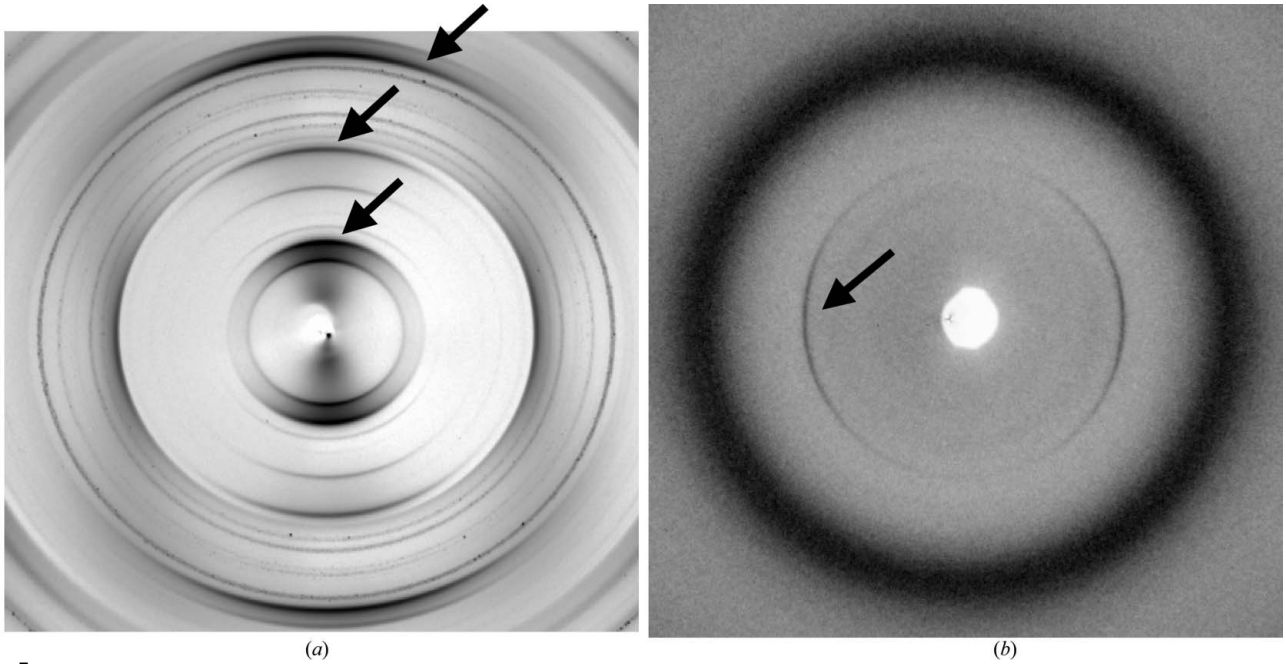

(*a*) (*b*)

**Figure 5**
Centre parts of two-dimensional scattering images obtained from the anisotropic powders of clay nano-stacks. The anisotropic rings used to infer the orientation distributions of the crystallites are indicated by arrows. (*a*) Picture obtained from dry-pressed samples. The camera length was 375 mm. (*b*) Picture from electrorheological chains of crystallites in oil. The camera length was 376 mm. The anisotropic ring in the centre of (*b*) is the (001) ring for the nano-stack structure in the 1WL hydration state. Its anisotropy is orthogonal to that observed in (*a*). The image magnification is 1.5 with respect to (*a*). The broad peak outside the (001) ring is due to diffuse scattering from the silicon oil.

**Table 1**
Characteristic momentum transfer ($q$) and length scales ($d$) measured for the 0WL diffraction peaks from dry-pressed samples of Na fluorohectorite.

| | 0WL(001) | 0WL(002) | 0WL(003) |
|---|---|---|---|
| $q$ (nm$^{-1}$) | 6.50 ± 0.03 | 13.02 ± 0.03 | 19.57 ± 0.03 |
| $d$ (Å) | 9.67 ± 0.04 | 9.65 ± 0.03 | 9.63 ± 0.03 |

(New York). The raw powder was carefully cation-exchanged so as to force the replacement of all intercalated cations by $Na^+$ (Løvoll *et al.*, 2005). The resulting wet gel was then suspended in deionized water again, and after sufficient stirring time, water was expelled by applying a uniaxial load in a hydrostatic press. The resulting dry assembly was then cut in strips of 4 mm by 47 mm.

The resulting samples are anisotropic, with a marked average alignment of the clay crystallites parallel to the horizontal plane (Knudsen *et al.*, 2004), as shown in the two-dimensional sketch of the sample geometry, in the inset to Fig. 4. A nematic description such as that presented in section §2.2.1, with a mean director $\mathbf{n}_0$ close to the direction of the applied uniaxial load, describes their geometry well.

### 3.3. Experimental setup

Two-dimensional diffractograms of dry-pressed samples were obtained on beamline BM01A at the European Synchrotron Radiation Facility (ESRF) in Grenoble (France). Fig. 4 shows a simplified sketch of the experimental geometry; the sample cell allowing humidity and temperature control in the surrounding atmosphere is not shown. A more complete description of the sample environment can be found in work by Méheust, Fossum *et al.* (2005). We used a focused beam of width 0.5 mm with energy 17.46 keV, corresponding to a wavelength of 0.71 Å. The scattering images were recorded using a two-dimensional MAR345 detector, with a resolution of 2300 pixels across the diameter of the circular detector (width 345 mm). The distance between the sample and the detector was calibrated to 375.25 mm using a silicon powder standard sample (NBS640b).

The 5 × 2× 1 mm samples were positioned with the average nano-stack director close to vertical. The path length of the beam through the samples was ∼2 mm, resulting in a scattering volume of ∼0.4 mm$^3$. Taking into account the typical crystallite volume (0.1 µm$^3$) and the sample porosity [between 40 and 50% (Knudsen *et al.*, 2004)], we estimate the number of crystallites in the scattering volume to ∼2 × 10$^9$. Thus, the assumption according to which the entire size and orientation distribution are contained in the scattering volume (see §2.1) is reasonable.

### 3.4. Image analysis

The centre part of a two-dimensional scattering image obtained from a dry-pressed Na fluorohectorite sample at a temperature of 370.7 K is shown in Fig. 5(*a*). The image anisotropy appears clearly, with a much stronger intensity of some of the diffraction rings along the vertical direction. Some grainy-looking isotropic rings can also be seen; they are due to impurities (mostly mica). In what follows, we infer the orientation distribution for the clay crystallites from three rings, separately. These rings correspond to the first three orders of the same reflection.

**3.4.1. Method**. The images were analyzed in the following way. After finding the image centre (incident-beam direction), we compute diffraction lines at azimuthal angle values $\varphi_m$, varying $\varphi_m$ between 0 and 359° by steps of 1°. For a given value of $\varphi_m$, the diffraction line is obtained by integrating over $\varphi$ the image subpart corresponding to values of $\varphi$ in the range

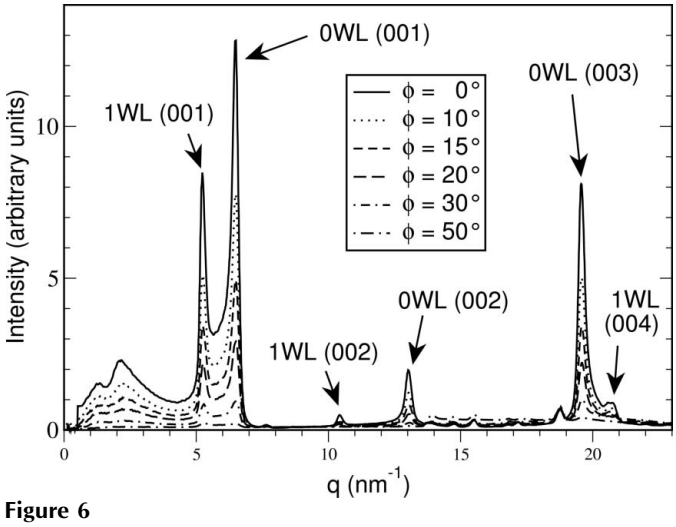


**Figure 6**
Powder diffraction profiles recorded along different azimuthal directions on the two-dimensional detector, with a dry-pressed sample at $T$ = 371 K. Several peaks characteristic of the nano-layered structure of the crystallites are visible. Their intensity decreases dramatically as $\varphi$ increases due to the decrease of the number of crystallites that meet the Bragg condition at these angles.

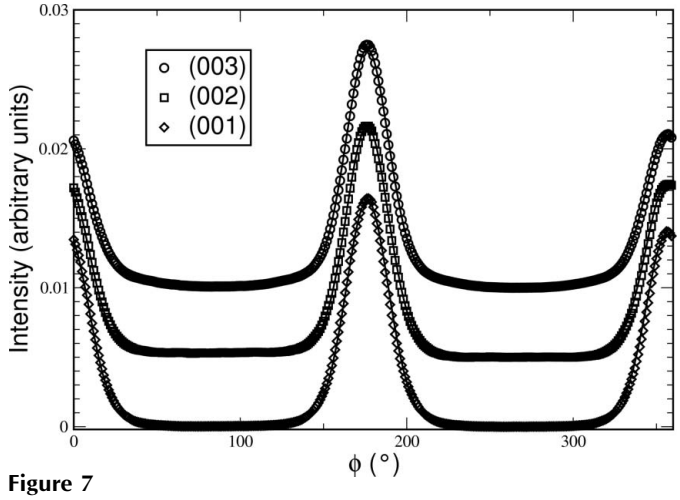


**Figure 7**
Azimuthal profiles observed from the scattering of dry-pressed samples at three values of $q$ corresponding to the first three orders of reflection by the population of crystallites in the 0WL hydration state. The profiles have been normalized and translated vertically for clarity. The fits according to equation (15) are shown as solid lines.

**Table 2**
Values obtained for the fit parameters $m$, $\Theta_0$ and $\Phi_0$, and for the angular width $w_f$ and order parameter $S$.

'Dry' denotes the dry-pressed Na fluorohectorite samples, while 'ER' denotes the electrorheological bundles of Na fluorohectorite particles.

| | Dry (001) | Dry (002) | Dry (003) | ER (001) |
|---|---|---|---|---|
| $m$ | 10.45 ± 0.06 | 10.21 ± 0.27 | 10.21 ± 0.13 | 3.10 ± 0.23 |
| $w_f/2$ | 19.10 ± 0.07 | 19.38 ± 0.33 | 19.37 ± 0.16 | 24.48 ± 0.50 |
| $S$ | 0.85 ± 0.01 | 0.85 ± 0.01 | 0.84 ± 0.01 | 0.56 ± 0.02 |
| $\Theta_0$ | 6.12 ± 0.04 | 5.57 ± 0.10 | 5.87 ± 0.05 | −1.64 ± 0.05 |
| $\Phi_0$ | 176.37 ± 0.01 | 176.32 ± 0.01 | 176.37 ± 0.02 | 267.74 ± 0.02 |

$[\varphi_m - \delta\varphi/2;\ \varphi_m + \delta\varphi/2]$, where $\delta\varphi = 5^\circ$. Six of these powder diffraction profiles are shown in Fig. 6. They exhibit six peaks characteristic of the nano-layered structure of the crystallites: the first three orders for the population of crystallites with no water layer intercalated (0WL), and the orders 1, 2 and 4 for the population of crystallites with one water layer intercalated (1WL . . . ). At this temperature, the 1WL state is unstable (da Silva *et al.*, 2003); it is present in these pictures because the transition between the two hydration states has not finished yet. The analysis is carried out on the peaks 0WL(001), 0WL(002) and 0WL(003), which are the most intense, and are weakly perturbed by other peaks. The corresponding characteristic length scales are listed in Table 1; they are in good agreement with previous measurements (da Silva *et al.*, 2002).

For each of the three peaks 0WL(001), 0WL(002) and 0WL(003), the peak's intensity at maximum was plotted as a function of $\varphi$, and the obtained profiles were fitted with equation (6). The three normalized profiles are shown in Fig. 7; they have been translated vertically for clarity. As a functional form for the orientation distribution, we chose the Maier–Saupe function [equation (14)]. We also allowed a constant background $I_0$ to be accounted for. This resulted in fitting to the profiles a function of the form [using equations (6) and (14)]

$$I_0 + C\exp\left\{m\left[\sin\theta\sin\Theta_0 + \cos\theta\cos\Theta_0\cos(\varphi - \Phi_0)\right]^2\right\}, \tag{15}$$

with fitting parameters $I_0$, $C$, $m$, $\Theta_0$ and $\Phi_0$. Using the fitted model, we then derived the quantities characteristic of the orientational ordering in the samples, namely the order parameter $S$ [equation (8)] and the angular RMS width $w_f$ [equation (9)].

Note that (i) equation (15) depends on the diffraction peak chosen, as the value for the half scattering angle $\theta$ is not a fitting parameter but is different for each of the three profiles. (ii) Since the effect of sample absorption on scattered intensities consists of a slowly varying modulation with $2\theta$, it is independent of the azimuthal angle and only impacts on the overall amplitude of azimuthal profiles. Hence, it is contained in the proportionality constant of equation (6), and consequently in the fitting parameter $C$ in equation (15). (iii) As each of the fit parameters controls a particular shape aspect of the profiles (see §2.3), we can derive estimates for the parameters $I_0$, $C$, $m$, $\Theta_0$ and $\Phi_0$, using a few approximations (see Appendix *A*), and use these estimates as initial parameters for the fits. The fitting procedure is fast and the fitted parameters do not depend on the initial guesses.

**3.4.2. Results**. The fits are shown in Fig. 7 as solid lines, on top of the data points. For each fit, the standard statistical confidence ranges for each fitted parameter were computed. We also estimated an uncertainty of the fitted parameters from the fluctuations in their values obtained by varying the range of data points (between 30 and 90° from the peaks) considered for the fit. This method provided uncertainty values that were considerably larger than the statistical confidence ranges obtained for each fit. Consequently, those large uncertainty values were used as final estimates of the uncertainties of our parameters. They arise from two effects. The first effect is the deviation between the data profiles and the model used to fit them: if the two shapes are different, the parameters obtained by fitting the latter to the former will depend on the data range chosen for the fit. The second effect is the influence of the noise on the fitted parameters: as $\varphi$ moves away from the peak values $\Phi_0$ and $\Phi_0 + \pi/2$, and as the intensity decreases to the noise level of the diffraction profiles shown in Fig. 6, the significance of the intensity $I(\varphi)$ in terms of orientation distribution of the profiles is somewhat diluted. Thus, the points in the flat sections outside the peaks in Fig. 7 are of little relevance when fitting the model to the data. This effect is responsible for reflections with a higher order, and therefore smaller amplitude, displaying larger errors of the fitted parameters.

For each of the profiles, the fitted parameters and the derived quantities are shown in Table 2. The results obtained from the different orders are consistent with each other within the uncertainties, except for the parameter $\Theta_0$ where a 0.5° discrepancy exists. This is, however, small, and the first-order profile was expected to behave slightly differently from the others as the corresponding peak is not totally separated from the 1WL(001) peaks (see Fig. 6). This profile also gives a value for the angular width that is slightly different, but consistent with the other orders within the error bars. We can thus estimate the average orientation of the nano-stack population to $(\Theta_0,\Phi_0) = (5.8 \pm 0.5^\circ; 176.3 \pm 0.1^\circ)$. This value results from a possible non-parallelism of the average crystallite orientation from the direction of the constraint applied during sample preparation, and from a possible misalignment of the sample (a few degrees at most) from the horizontal direction.

## 4. Application to an antinematic configuration

We now apply the technique to data obtained in WAXS experiments with bundles of Na fluorohectorite particles in silicon oil.

### 4.1. Electorheological chains of fluorohectorite particles

Fluorohectorite samples were prepared by suspending 1.5% by weight of clay particles in silicon oil (Rothiterm M150, with a viscosity of 0.1 Pa s at 298 K). The hydration state of the particles prior to suspension in the oil was 1WL. When an

electric field above 500 V mm$^{-1}$ was applied, the suspended crystallites polarize, and the subsequent induced dipoles interact with each other, leading to aggregation of the clay crystallites in columnar bundles (Fossum *et al.*, 2006). This can be seen in the microscopy picture shown in Fig. 8. These bundles are on average parallel to the applied electric field.

### 4.2. Experimental setup

The orientation of the polarized crystallites inside the bundles was investigated using synchrotron WAXS. A top view of the experimental setup is sketched in Fig. 9: the suspensions were contained in a sample cell between two vertical copper electrodes separated by a 2 mm gap. A 1 kV electric field was applied between the electrodes. Horizontal bundles of polarized particles were observed to form within 20 s after the field was switched on, and two-dimensional diffractograms were recorded after formation of the bundles.

The experiments were performed at the Swiss–Norwegian Beamlines at ESRF, using the same beam energy and detector as presented in §3.3, the same beam diameter of 0.5 mm, and a path length in the sample of 1 mm. The sample's density in solid particles, in the absence of an electric field, was ∼2% by volume, corresponding to 20–25 times less scatterers per volume than in the dry-pressed samples. Hence, the scattering volume contained a very large ($> 10^8$) number of crystallites. After the electric field had aggregated clay particles together, the number of particles in the scattering volume was even larger, which is confirmed by the intense and continuous (anisotropic) scattering rings observed.

### 4.3. Image analysis

Fig. 5(*b*) displays the centre of a scattering image obtained after the chains have settled in the electric field. These WAXS data contain a significant background, with a broad ring due to diffuse scattering from the oil, but the 1WL(001) peak characteristic of the nano-layered structure of the crystallites is clearly visible. It is observed to be much more intense along the horizontal direction, which means that the directors of the crystallites are, on average, in a plane perpendicular to the direction of the bundle (Fossum *et al.*, 2006). Furthermore, an axial symmetry around the horizontal direction perpendicular to the X-ray beam, that is, around the average direction for the bundles, is expected. Thus, the antinematic description presented in §2.2.2 is well suited to describe the orientational ordering in the chains.

**4.3.1. Method**. The image analysis was performed in exactly the same way as for the nematic geometry studied previously. It was carried out on the ring corresponding to the first-order reflection for the 1WL hydration state, as shown by the arrow in Fig. 5(*b*). The choice of a Maier–Saupe functional form for the orientation distribution is not only phenomenological here. Indeed, this precise shape is expected in a system of identical induced dipoles where alignment by an external field competes with the homogenizing entropy (Fossum *et al.*, 2006; Méheust, Parmar *et al.*, 2005).

**4.3.2. Results**. The normalized azimuthal profile extracted from the two-dimensional scattering image is shown in Fig. 10, with the corresponding model fitted over the whole range of azimuthal angles. Despite a significant noise away from the peak positions, the fit is satisfying. The uncertainties of the angular RMS width and order parameters (see Table 2, column marked ER) are estimated in the way described in §3.4.2.

**Figure 8**
Close view of a chain formed under the application of a strong electric field by Na fluorohectorite crystallites suspended in silicon oil. The original colour image has been filtered. The gap between the electrodes, the boundaries of which are shown by two vertical bold lines on the sides of the picture, is 2 mm.

## 5. Discussion

Our populations of nano-layered crystallites are statistically invariant over rotations around the reference direction $\mathbf{n}_0$. This invariance bears some resemblance to the symmetries

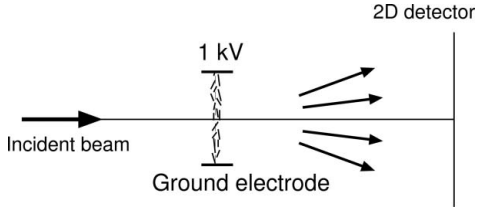


**Figure 9**
Top view of the experimental scattering geometry used to scatter X-rays by electrorheological chains of Na fluorohectorite crystallites. The electrodes are vertical and the chains of aggregated crystallites are along a direction that is close to perpendicular to the electrodes. The disorder in the chains is exaggerated in this sketch.

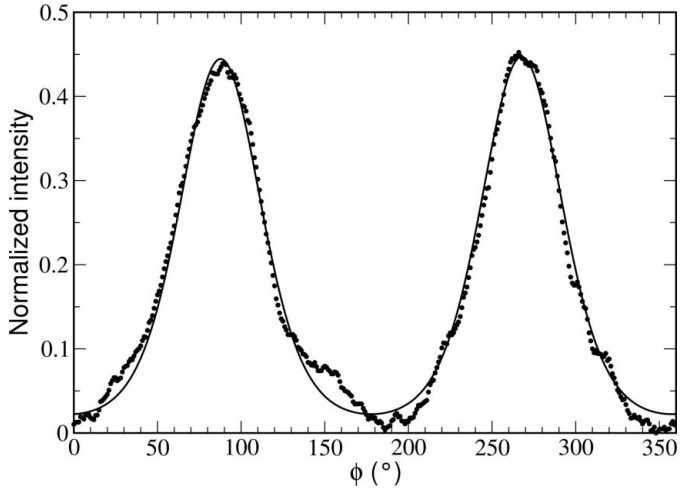


**Figure 10**
Azimuthal profile at $q = 5 \times 10$ nm$^{-1}$, corresponding to the 001 peak of Na fluorohectorite in the 1WL hydration state. The corresponding fit is plotted as a solid line.

observed in fibre systems. However, the detail of the latter symmetries is usually quite complex. The three-dimensional structure of the scattering system has to be considered when addressing such fibre systems, and the treatment of fibre diffraction data is often quite complicated (Fraser *et al.*, 1976). In this paper, taking advantage of the one-dimensional diffraction by the clay nano-stacks, and of the axial symmetry of their ODP function, we have been able to derive a simple procedure to infer the ODP from two-dimensional WAXS images.

This procedure has several strong points with respect to techniques commonly used for such nano-stack systems and based on a one-dimensional recording (the 'rocking-curve' technique, for example). The first benefit is that the method requires very little data acquisition time, since only one recording is necessary. Such a recording can be obtained in a couple of minutes at a third-generation synchrotron source. It therefore allows *in situ* measurements of the orientation distribution while changing experimental parameters. In the two examples given here, it could be the surrounding humidity and the magnitude of the applied electric field, respectively. The second benefit is that it allows determination of the reference orientation in the three dimensions of space. The rocking-curve method provides the inclination $\Theta_0$ of that direction with respect to planes normal to the incident beam in the case where $\Phi_0 = 0$ only. It does not intrinsically provide correct estimates of the angles $\Theta_0$ and $\Phi_0$ without prior time-consuming adjustment of the sample azimuthal orientation so as to ensure the condition $\Phi_0 = 0$. Moreover, it introduces a bias in the estimated width of the orientation distribution in the case where $\Phi_0 \neq 0$.

We determine an uncertainty on the inferred ordering parameters from the dispersion of the fitted values when changing the range of azimuth angles used for the fit. This uncertainty is larger than the statistical confidence range provided by the fitting procedure for a given range of azimuth angles; it is, to a certain extent, a measure of how good the modelled profile shape is suited to the experimental profile, but is also influenced by the noise level of the scattering image; the process is more trustworthy if the diffraction peak considered is more intense. How the accuracy of the method depends on the peak's intensity with respect to the noise level is not quantified here. How the vicinity of another peak to the peak used to determine $f$, as in the 0WL(001) peak in §3, modifies the azimuthal profiles, is not known quantitatively either, and we propose that our method is accurate when applied to a reflection whose peak is well separated from other peaks. Despite those shortcomings, we think the method has several advantages over the rocking-curve method and allows a better description of the orientational order in the samples, because (i) the reference direction $\mathbf{n}$ is determined, (ii) no bias in the angular width is introduced in the case where $\mathbf{n}_0$ does not coincide with the $O\mathbf{z}$ direction of the laboratory frame, (iii) an uncertainty is determined during the fitting procedure, for each azimuthal profile considered, and (iv) measurement consistency can be checked by comparing the results obtained from several different azimuthal profiles corresponding to several different diffraction peaks, on the same single recording. Finally, the method is easily carried out practically, since the only mathematical procedure involved is the fitting of equation (6) to azimuthal profiles.

## 6. Conclusion and prospects

We have developed a method to determine orientation distributions in anisotropic powders of nano-layered crystallites from a single two-dimensional scattering image, in the case when the orientation distribution only depends on the deviation from a reference direction. The method relies on fitting the proper relation to the azimuthal decay of a given diffraction peak's amplitude. It allows determination of the reference direction and of the angular dispersion of the distribution. It was applied successfully to data obtained from two synchrotron X-ray scattering experiments, on two different systems of synthetic smectite clay particles where the particle assemblies exhibit a nematic and antinematic ordering, respectively. In the first case, the consistency of the inferred quantities was checked by comparing the results obtained from three different orders of the same reflection.

The method is promising as it is performed on a single two-dimensional recording, and therefore allows *in situ* determination of orientational ordering in samples when thermodynamical conditions are varying. It shall be used in this respect in the future.

## APPENDIX *A*
## Initial parameters for the fits

The initial parameters for the fitting function in the form (15) are set to prior estimates of those parameters. The prior estimates are obtained from the data profiles using a few approximations, as explained below.

The parameter $I_0^{(i)}$ is first estimated as the minimum value of the data plot. A running average is performed on the data in order to smooth out the noise and obtain a curve with only two maxima: those corresponding to the peaks. The value for $\Phi_0^{(i)}$ is set to the azimuthal position of the largest peak. Its peak intensity, $I_1$, and that of the second peak, $I_2$, are determined. The half-width at half-maximum $w$ of the largest peak is estimated numerically. The parameter $m^{(i)}$ is then defined from $w$ by stating:

$$\exp(m^{(i)} \cos^2 w) = \exp(m^{(i)})/2, \tag{16}$$

which provides the relation

$$m^{(i)} = (\ln 2)/(1 - \cos^2 w). \tag{17}$$

The maxima $I_1$ and $I_2$ are obtained for $\varphi = \Phi_0$ and $\varphi = \Phi_0 + \pi$; hence one can state:

$$\begin{cases} I_1 - I_0^{(i)} = C \exp\left[m^{(i)} \cos^2(\theta - \Theta_0^{(i)})\right], \\ I_2 - I_0^{(i)} = C \exp\left[m^{(i)} \cos^2(\theta + \Theta_0^{(i)})\right]. \end{cases} \tag{18}$$

From this, it follows that

$$\ln\left(\frac{I_1 - I_0^{(i)}}{I_2 - I_0^{(i)}}\right) = m^{(i)} \sin(2\theta) \sin(2\Theta_0^{(i)}). \quad (19)$$

from which an estimate of $\Theta_0$ is obtained:

$$\Theta_0^{(i)} = \frac{1}{2} \operatorname{Asin}\left[\frac{1}{m^{(i)} \sin(2\theta)} \ln\left(\frac{I_1 - y_0^{(i)}}{I_2 - y_0^{(i)}}\right)\right]. \quad (20)$$

Finally, going back to equation (18), we obtain $C^{(i)}$ in the form

$$C^{(i)} = \frac{I_1 - y_0^{(i)}}{\exp\left[m^{(i)} \cos^2(\theta - \Theta_0^{(i)})\right]}. \quad (21)$$

The staff at the Swiss–Norwegian Beamlines at ESRF are gratefully acknowledged for support during the synchrotron experiment. We also thank the two anonymous referees for helping to improve the paper. This work was supported by the Norwegian Research Council (NRC), through the research grants numbers 152426/431, 154059/420 and 148865/432.

## References

Bunge, H.-J. (1993). *Texture Analysis in Materials Science.* Göttingen: Cuvillier Verlag.
Courville, J. de, Tchoubar, D. & Tchoubar, C. (1979). *J. Appl. Cryst.* **12**, 332–338.
DiMasi, E., Fossum, J. O., Gog, T. & Venkataraman, C. (2001). *Phys. Rev. E*, **64**, 061704.
Drits, V. A. & Tchoubar, C. (1990). *X-ray Diffraction by Disordered Lamellar Structures*, ch. 2, pp. 40–42. Berlin: Springer Verlag.
Fossum, J. O., Méheust, Y., Parmar, K. P. S., Knudsen, K. D. & Måløy, K. J. (2006). *Europhys. Lett.* In the press.
Fraser, R. D. B., Macrae, T. P., Miller, A. & Rowlands, R. J. (1976). *J. Appl. Cryst.* **9**, 81.
Gennes, P. G. de & Prost, J. (1993). *The Physics of Liquid Crystals*, 2nd ed., ch. 2.1, pp. 41–42. Oxford: Oxford Science Publications.
Güntert, O. J. & Cvikevich, S. (1964). *Carbon*, **1**, 309–313.
Ischia, G., Wenk, H.-R., Lutterotti, L. & Berberich, F. (2005). *J. Appl. Cryst.* **38**, 377–380.
Kaviratna, P. D., Pinnavaia, T. J. & Schroeder, P. A. (1996). *J. Phys. Chem. Solids*, **57**, 1897–1906.
Knudsen, K. D., Fossum, J. O., Helgesen, G. & Haakestad, M. W. (2004). *Physica B*, **352**, 247–258.
Lasocha, W. & Schenk, H. (1997). *J. Appl. Cryst.* **30**, 561–564.
Løvoll, G., Sandnes, B., Méheust, Y., da Silva, G. J., Mundim, M. S. P., Droppa, R. & Fonseca, D. d. M. (2005). *Physica B.* Accepted.
Maier, W. & Saupe, A. (1958). *Z. Naturforsch. A*, **13**, 564–566.
Maier, W. & Saupe, A. (1959). *Z. Naturforsch. A*, **14**, 882–889.
Méheust, Y., Fossum, J. O., Knudsen, K. D., Måløy, K. J. & Helgesen, G. (2005). *Mesostructural changes in a Clay intercalation compound during hydration transitions*. In preparation.
Méheust, Y., Parmar, K., Fossum, J. O., Fonseca, D. d. M., Knudsen, G. & Måløy, K. J. (2005). *Orientational ordering inside electrorheological chains of nano-silicate particles in silicon oil – a WAXS study*. In preparation.
Plançon, A. (1980). *J. App. Cryst.* **13**, 524–528.
Puig-Molina, A., Wenk, H.-R., Berberich, F. & Graafsma, H. (2003). *Z. Metallkdd.* **94**, 1199–1205.
Silva, G. J. da, Fossum, J. O. & DiMasi, E. (2002). *Phys. Rev. E*, **66**, 011303.
Silva, G. J. da, Fossum, J., DiMasi, E. & Måløy, K. J. (2003). *Phys. Rev. B*, **67**, 094114.
Taylor, R. M. & Norrish, K. (1966). *Clay Miner.* **6**, 127–141.
Velde, B. (1992). Editor. *Origin and Mineralogy of Clays.* London: Chapman and Hall.
Wada, N., Hines, D. R. & Ahrenkiel, S. P. (1990). *Phys. Rev. B*, **41**, 12895–12901.
Wenk, H.-R. (1985). Editor. *Preferred Orientation in Deformed Metals and Rocks: An Introduction to Modern Texture Analysis.* London: Academic Press.
Wenk, H.-R. & Grigull, S. (2003). *J. Appl. Cryst.* **36**, 1040–1049.
Wessels, T., Baerlocher, C. & McCusker, L. B. (1999). *Science*, **284**, 477–479.